NASA/TM-2001-211248

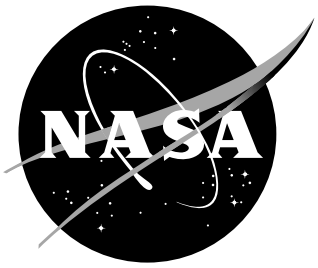

The Effect of O_2, H_2O, and N_2 on the Fatigue Crack Growth Behavior of an $\alpha+\beta$ Titanium Alloy at 24 °C and 177 °C

Stephen W. Smith and Robert S. Piascik
Langley Research Center, Hampton, Virginia

December 2001

The NASA STI Program Office ... in Profile

Since its founding, NASA has been dedicated to the advancement of aeronautics and space science. The NASA Scientific and Technical Information (STI) Program Office plays a key part in helping NASA maintain this important role.

The NASA STI Program Office is operated by Langley Research Center, the lead center for NASA's scientific and technical information. The NASA STI Program Office provides access to the NASA STI Database, the largest collection of aeronautical and space science STI in the world. The Program Office is also NASA's institutional mechanism for disseminating the results of its research and development activities. These results are published by NASA in the NASA STI Report Series, which includes the following report types:

- TECHNICAL PUBLICATION. Reports of completed research or a major significant phase of research that present the results of NASA programs and include extensive data or theoretical analysis. Includes compilations of significant scientific and technical data and information deemed to be of continuing reference value. NASA counterpart of peer-reviewed formal professional papers, but having less stringent limitations on manuscript length and extent of graphic presentations.

- TECHNICAL MEMORANDUM. Scientific and technical findings that are preliminary or of specialized interest, e.g., quick release reports, working papers, and bibliographies that contain minimal annotation. Does not contain extensive analysis.

- CONTRACTOR REPORT. Scientific and technical findings by NASA-sponsored contractors and grantees.

- CONFERENCE PUBLICATION. Collected papers from scientific and technical conferences, symposia, seminars, or other meetings sponsored or co-sponsored by NASA.

- SPECIAL PUBLICATION. Scientific, technical, or historical information from NASA programs, projects, and missions, often concerned with subjects having substantial public interest.

- TECHNICAL TRANSLATION. English-language translations of foreign scientific and technical material pertinent to NASA's mission.

Specialized services that complement the STI Program Office's diverse offerings include creating custom thesauri, building customized databases, organizing and publishing research results ... even providing videos.

For more information about the NASA STI Program Office, see the following:

- Access the NASA STI Program Home Page at ***http://www.sti.nasa.gov***

- E-mail your question via the Internet to help@sti.nasa.gov

- Fax your question to the NASA STI Help Desk at (301) 621-0134

- Phone the NASA STI Help Desk at (301) 621-0390

- Write to:
  NASA STI Help Desk
  NASA Center for AeroSpace Information
  7121 Standard Drive
  Hanover, MD 21076-1320

NASA/TM-2001-211248

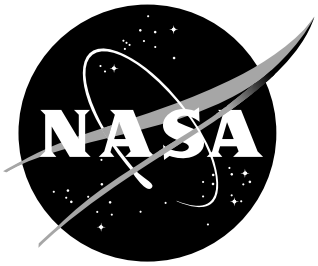

The Effect of O_2, H_2O, and N_2 on the Fatigue Crack Growth Behavior of an $\alpha+\beta$ Titanium Alloy at 24 °C and 177 °C

Stephen W. Smith and Robert S. Piascik
Langley Research Center, Hampton, Virginia

National Aeronautics and
Space Administration

Langley Research Center
Hampton, Virginia 23681-2199

December 2001

Acknowledgments

The authors gratefully acknowledge Dr. Steven Yu of the Naval Research Laboratory for performing the XPS analysis.

Available from:

NASA Center for AeroSpace Information (CASI)
7121 Standard Drive
Hanover, MD 21076-1320
(301) 621-0390

National Technical Information Service (NTIS)
5285 Port Royal Road
Springfield, VA 22161-2171
(703) 605-6000

List of Symbols:

a	crack length
Δa	crack length increment
da/dN	fatigue crack growth rate
E	elastic modulus
EC(T)	extended compact tension
ESE(T)	eccentrically-loaded single edge tension
k	Boltzmann's constant
K	stress-intensity factor
K_{max}	maximum stress-intensity factor
K_{min}	minimum stress-intensity factor
K_{mean}	mean stress-intensity factor $((K_{max} + K_{min})/2)$
K_{op}	opening stress-intensity factor
ΔK	cyclic stress-intensity factor $(K_{max} - K_{min})$
ΔK_{eff}	effective cyclic stress-intensity factor $(K_{max} - K_{op})$
ΔK_{th}	threshold cyclic stress-intensity factor
M	molecular weight
N	fatigue cycles
$\dot{n}$	adsorption rate of a gaseous specie on a crack surface
P_{crit}	pressure required for the adsorption of one monolayer on a crack surface
Prob	sticking probability for a gaseous specie on a crack surface
QMS	quadrupole mass spectrometer
R	stress ratio (K_{min} / K_{max})
T	temperature
t	time
UHV	ultra high vacuum
$\dot{V}$	volumetric flow rate of a gas to a crack tip
XPS	X-ray Photoelectron Spectroscopy
$\delta(x)$	crack opening at a distance x from the crack tip
σ_o	flow stress
ν	average gas velocity

Abstract

To study the effects of atmospheric species on the fatigue crack growth behavior of an α+β titanium alloy (Ti 6-2-2-2-2) at room temperature and 177 °C, fatigue tests were performed in laboratory air, ultrahigh vacuum, and high purity water vapor, oxygen, nitrogen and helium at various partial pressures. Accelerated fatigue crack growth rates in laboratory air compared to ultrahigh vacuum are linked to the damaging effects of both water vapor and oxygen. Observations of the fatigue crack growth behavior in ultrahigh purity environments, along with surface film analysis using X-ray photoelectron spectroscopy (XPS), suggest that multiple crack-tip processes govern the damaging effects of air. Three possible mechanisms are proposed: 1) at low pressure (< 10^{-1} Pa), accelerated da/dN is likely due to monolayer adsorption on crack-tip surfaces presumably resulting in decreased bond strengths at the fatigue crack tip, 2) for pressures greater than 10^{-1} Pa, accelerated da/dN in oxygen may result from oxidation at the crack tip limiting reversible slip, and 3) in water vapor, absorption of atomic hydrogen at the reactive crack tip resulting in process zone embrittlement.

Introduction

A fundamental understanding of crack-tip damage mechanisms is required for the development of robust airframe damage tolerant life prediction methodology. New titanium alloys are being considered for use in future high-speed airframes due to improved stiffness, toughness and specific strength as compared to conventional alloys such as Ti 6Al-4V. The corrosion resistance properties of titanium alloys are a result of stable surface oxides. However, growing fatigue cracks continuously breach the protective oxide layer exposing the highly reactive crack tip to environmental attack. In order to develop reliable fracture mechanics based life predictions for titanium alloy structures, crack tip environmental damage mechanisms must be understood.

Although numerous studies have shown that ambient air is a damaging environment for components subjected to fatigue loading, damage processes are not well understood [1-4]. This is particularly true for titanium and titanium alloys. While researchers have shown that the presence of water vapor results in accelerated damage in titanium alloys [5, 6], the mechanisms associated with environmentally assisted cracking in air are not well known. The influence of atmospheric species other than water vapor (namely oxygen) has not been adequately addressed. This paper presents a systematic study that identifies the damaging species and possible damage mechanisms affecting the growth of fatigue cracks in a titanium alloy exposed to air at temperatures from 24 °C to 177 °C.

Material and Experimental

The α+β titanium alloy studied, Ti 6-2-2-2-2 (Ti-5.60 Al-1.81 Zr-1.79 Cr-1.88 Sn-1.96 Mo-0.23 Si, wt.%) was received in sheet form cross rolled to a final thickness of 1.65 mm (0.065 inch).

The alloy was hot rolled at 927 °C (1700 °F) and solution annealed at 899 °C (1650 °F) for 30 minutes, followed by an aging treatment at 510 °C (950 °F) for 10 hours (the material was processed in packs of several sheets which were air cooled following all heat treatments). The solution treated and aged product contained primary α grains less than 10 μm, with transformed β colonies.

All fatigue crack growth rate testing was performed using closed loop servo-hydraulic machines, operated under load control, with sinusoidal waveform loading. Laboratory air and vacuum tests were conducted at room temperature (24°C) and 177 °C. Controlled environmental testing was performed in a metal-to-metal sealed stainless steel vacuum chamber (Figure 1). High purity gaseous environments were created by first evacuating the vacuum chamber to ultrahigh vacuum (UHV), less than 7×10^{-7} Pa, then introducing high purity O_2, N_2, He or water vapor.

The purity of the testing environment was monitored using a quadrupole mass spectrometer (QMS) located in the vacuum test chamber and a second QMS located in a differentially pumped vacuum chamber (shown in Figure 1b). For total pressures less than 1×10^{-2} Pa, partial pressure analysis was performed using the QMS within the test chamber. At higher total pressures, a series of orifice valves were used to meter small quantities of the test environment into the differentially pumped vacuum chamber for analysis (see Figure 1b). Typical mass spectral scans are shown for high purity water vapor (Figure 2) and oxygen (Figure 3) environments. The partial pressures of the major constituents were calculated from the spectral data and are shown in Tables I and II.

Eccentrically-loaded single edge crack tension (ESE(T)) specimens (formerly known as extended compact tension, EC(T) specimens) [7] (see Figure 4) were machined in the T-L orientation and used for fatigue crack growth rate testing. All testing was performed under stress-intensity factor (K) control, using a computer-based system. The back-face strain gage compliance technique was used to determine crack lengths and load-displacement measurements were used to determine crack-tip closure [7-9]. Visual crack length measurements were performed periodically during fatigue testing and were used along with a final fracture surface crack length to make small (typically 0.5% error) corrections (by linear interpolation) to the compliance based crack length determinations.

Variable ΔK and constant ΔK tests were performed in accordance with ASTM standard E 647 [8]. All tests were conducted at $R = 0.5$ or 0.75. No crack-tip closure was observed at these stress ratios using either the ASTM offset technique [8] or Elber's reduced displacement technique [9]. Constant ΔK tests were performed to accurately quantify the influence of environment on fatigue crack growth rate (da/dN) by monitoring steady-state da/dN for each controlled environment. Steady-state conditions are defined as a constant slope of the crack length (a) versus fatigue cycle (N) data for fatigue crack length intervals (Δa) greater than 0.6 mm. As the environment was changed under constant ΔK conditions, corresponding changes in slope of the a versus N plot accurately quantified the influence of the environment on fatigue crack growth. An example of data acquired using this technique is shown in Figure 5. Here, four regions of nearly equivalent steady-state crack growth rates are identified for different environments (seven high purity oxygen pressures and UHV).

The fatigue crack surfaces of selected samples were examined using X-ray photoelectron spectroscopy (XPS) [10]. Each specimen was removed from the fatigue test chamber and stored in a container backfilled with dry helium prior to examining the fatigue surfaces using XPS. X-ray excited O^{1s} photoelectrons (ranging from 525 to 539 eV) from the fatigue crack surfaces were analyzed to determine the nature of oxygen on the fatigue crack surfaces. Previous studies have used XPS to correlate characteristic O^{1s} peaks with the formation of oxides, hydroxides and adsorbed water vapor on several metals when clean surfaces are exposed to oxygen and/or water vapor [11, 12]. It is acknowledged that contamination of the fatigue crack surfaces can occur between the time of fatigue testing and XPS analysis; however, observations about the nature of the fatigue crack surfaces will only be made by comparing surfaces produced under different exposure conditions that were handled similarly prior to

surface analysis.

Results

Initial tests were performed to quantify the damaging effects of air compared to an inert ultrahigh vacuum environment. A comparison of room temperature (24 °C) and elevated temperature (177 °C) fatigue crack growth behavior is shown in Figure 6 for laboratory air and UHV environments. Within the linear Paris regime (approximately 3.5 to 15 MPa√m for laboratory air and 6 to 15 MPa√m for UHV), fatigue crack growth rates in laboratory air are accelerated compared to UHV rates; for an applied ΔK of 10 MPa√m, a factor of four increase is observed at 24 °C and a factor of two increase is measured at 177 °C. A lower fatigue crack growth threshold was observed in laboratory air ($\Delta K_{th} \approx 2.1$ MPa√m) compared to UHV ($\Delta K_{th} \approx 4.0$ MPa√m)[1]. In laboratory air, fatigue crack growth rates are lower at elevated temperature, with the exception of the near threshold regime (ΔK < 4 MPa√m) where fatigue crack growth rates are nearly comparable. In UHV, little effect of elevated temperature is seen for ΔK < 17 MPa√m. For ΔK > 17 MPa√m, room temperature da/dN is accelerated compared to 177 °C da/dN in UHV. This suggests that temperature can affect the apparent toughness of Ti 6-2-2-2-2 [13]. However, over the range examined there is no effect of temperature on the fatigue crack growth behavior of Ti 6-2-2-2-2 in the Paris regime in the absence of an aggressive environment.

Purified Environments:

Constant ΔK tests were conducted at a ΔK of 6.6 MPa√m in pressure controlled purified environments. This value of ΔK was chosen because significant environmental effects were observed (lab air versus UHV) within the Paris regime where fatigue crack growth is well behaved (refer to dashed line in Figure 6). The following sections describe the results of tests conducted in high purity water vapor (H_2O), oxygen (O_2), nitrogen (N_2) and helium (He) at pressures ranging from approximately 10^{-3} Pa to 600 Pa. For reference, water vapor and oxygen partial pressures in 20% relative humidity air at 24 °C are approximately 590 Pa and 21,000 Pa, respectively.

Water Vapor Effects

Figure 7 describes the damaging effects of water vapor at 24 °C and 177 °C. These data are the results from twenty-nine constant ΔK tests and dashed lines are used to indicate the trends in the data. A comparison of multiple tests conducted at UHV (< 1 x 10^{-6} Pa) and at 10^{-3} Pa H_2O suggests a mild increase in inert fatigue crack growth rates at 24 °C compared to 177 °C. Over the range from UHV to a H_2O partial pressure of 10^{-2} Pa, no change in da/dN was observed at 24 °C or 177 °C. For H_2O pressures ranging from 10^{-2} to 10^{-1} Pa, a rapid increase in fatigue crack growth rate of more than factors of two and three were observed at room and elevated temperature, respectively. At 177 °C, a maximum da/dN is obtained for a pressure of approximately 10^{-1} Pa followed by a decrease in da/dN for pressures ranging from 10^{-1} Pa to about 4 Pa and then a slight increase at pressures greater than 4 Pa. In the pressure range from 4 Pa to 530 Pa, at 177°C, da/dN is approximately 25 % less than the rates in laboratory air and approximately 2.3 times greater than the rates in ultrahigh vacuum. At 24 °C, crack growth rates in high

[1] Threshold values are approximated at 1 x 10^{-10} m/cycle, as suggested in ASTM standard E 647 [8].

purity water vapor steadily approach laboratory air crack growth rates with increasing pressure from 10^{-1} to 530 Pa. At 530 Pa, da/dN is approximately 15 % less than the rates measured in laboratory air (≈ 35 to 70 % relative humidity (RH); at 50 % RH the water vapor partial pressure is approximately 1500 Pa) and approximately three times greater than the rates measured in ultrahigh vacuum at 24 °C.

Oxygen Effects

Figure 8 shows the damaging effect of molecular oxygen at 24 °C and 177 °C. The plot shows steady-state fatigue crack growth rates for thirty-three constant ΔK tests and dashed lines indicate the trends in the da/dN data. For oxygen pressures up to 10^{-2} Pa, da/dN remains the same as the rate at UHV. Fatigue crack growth rates increased for pressures greater than 10^{-2} Pa and reached a maximum at an oxygen pressure of approximately 10^{-1} Pa; here, room temperature oxygen da/dN is a factor of two greater than 24 °C UHV growth rates and 177 °C oxygen da/dN is a factor of three greater than 177 °C UHV growth rates. For pressures greater than 10^{-1} Pa and a temperature of 24°C, fatigue crack growth rates decrease with increasing pressure until a pressure of approximately 2 Pa is reached. Further increases in pressure up to 600 Pa result in a fairly constant crack growth rate that is approximately 1.5 times greater than da/dN in UHV at 24°C. For pressures greater than 10^{-1} Pa and a temperature of 177°C, a slight plateau in crack growth rate is observed up to a pressure of approximately 2 Pa. A further increase in pressure to 10 Pa results in a decrease in crack growth rate with increasing pressure followed by a fairly constant crack growth rate for pressures between 10 and 600 Pa. As was the case at 24°C, the fatigue crack growth rate for pressures between 10 and 600 Pa was approximately 1.5 times greater than the corresponding crack growth rate in UHV.

The formation of an oxide along newly created fatigue crack surfaces has been shown to be a potential source of crack closure [14-16]. To determine if the observed decrease in da/dN (for pressures greater than 10^{-1} Pa) is a result of oxide-induced closure, additional fatigue testing was performed at a higher stress ratio at 177°C. Figure 9 compares the results for two stress ratios (R = 0.5 and 0.75) in ultrahigh vacuum and high purity oxygen using steady-state fatigue crack growth rates for twenty-five constant ΔK tests. The trends are similar for the two values of R. Therefore, the same environmentally assisted mechanisms appear to be affecting the fatigue crack growth behavior at R = 0.5 and 0.75. For oxide-induced closure to affect the R = 0.75 data, the opening stress-intensity factor (K_{op}) would have to be greater than the minimum stress-intensity factor (K_{min} = 19.8 MPa$\sqrt{m}$). Because K_{op} is believed to be relatively constant in the Paris regime [17, 18], K_{op} would have to exceed the K_{max} at R = 0.5 (K_{max} = 13.2 MPa$\sqrt{m}$). Such a condition would lead to no fatigue crack growth at R = 0.5. This observation would tend to suggest that the decrease in da/dN for pressures greater than 10^{-1} Pa is not due to oxide induced crack closure. For the entire range of pressure examined, higher values of da/dN were obtained for R = 0.75 than for R = 0.5. This difference in crack growth rates is attributed to the difference in K_{max} at these two stress ratios as was concluded in a previous publication reporting tests in laboratory air [19]. It would appear that this is also true over the entire range of pressure shown in Figure 9.

Nitrogen and Helium Effects

Results show that nitrogen and helium do not directly affect the fatigue crack growth behavior of Ti 6-2-2-2-2. Specimens exposed to either of these gases at pressures from 10^{-1} Pa to 2 Pa at 24 °C and 177 °C exhibited roughly the same fatigue crack growth rate observed in UHV. These results also demonstrate that gaseous contaminants (namely water vapor) introduced during testing are minimal and do not lead to the accelerated fatigue crack growth behavior noted in Figures 7 or 8. One concern

during these tests was that adsorbed water on the surfaces near the specimen (namely the furnace) could be "scrubbed" by the introduction of gas at the pressures being used. This could result in an environment very near the specimen that was not consistent with that being measured at the mass spectrometer. Since the measured fatigue crack growth rate in nitrogen and helium were independent of pressure and consistent with rates measured in UHV, this form of contamination was not considered to be affecting any of the testing conditions.

Frequency Effects

The steady-state fatigue crack growth rate results for sixteen constant ΔK tests plotted in Figure 10 show the damaging effect of molecular oxygen at 24 °C and 177 °C at a loading frequency of 0.5 Hz. The trends in da/dN as a function of pressure are similar to those observed at a frequency of 5 Hz (Figure 8), with two exceptions: (1) the transitions in fatigue crack growth behavior occur at slightly lower pressure at f = 0.5 Hz compared to f = 5 Hz and (2) the maximum observed da/dN is higher for the lower frequency.

Analysis of Surface Films

Figure 11 shows O^{1s} photoelectron spectra for specimens fatigued in water vapor. The fatigue crack surfaces were produced in a high purity water vapor environment of 67 Pa. Each O^{1s} spectra (open circles in Figure 11) was curve fit using constituent gaussian peaks (dashed lines) and the sum of the constituent peaks is also presented (solid lines). At room temperature (Figure 11a) and 177 °C (Figure 11b), three constituent peaks are shown. Each constituent peak is in good agreement with published binding energies for oxygen associated with adsorbed water (533.5 eV), an hydroxide (532.0 eV) and an oxide (530.5 eV) (identified as dotted lines) [11, 12]. The height of the constituent peak identified as an hydroxide is approximately 4 times greater than the constituent peak for adsorbed water at room temperature and 177 °C. However, the relative height of the peak associated with an oxide is much greater at 177 °C than at 24 °C. This observation indicates that the surface is dominated by a hydroxide film in a water vapor environment at 24 °C; while at 177 °C an oxide can readily form, resulting in a surface film which consists of oxides and hydroxides.

Discussion

The fatigue crack growth behavior of Ti 6-2-2-2-2 is discussed in terms of three regions of pressure (I, II and III) for high purity water vapor (Figure 7) and oxygen Figures 8 through 10. A schematic of the observed behavior is shown in Figure 12. In the following discussion, the pressure range for each region will be identified for tests conducted at f = 5 Hz. While similar regions are observed at f = 0.5 Hz, the pressures are 2 to 5 times lower then those at f = 5 Hz. For pressures less than 1×10^{-2} Pa (Region I), no environmental effect on fatigue crack propagation is observed. Here, the da/dN in low-pressure H_2O or O_2 is similar to the da/dN in vacuum and inert helium.

Accelerated fatigue crack propagation in Region II may suggest that crack-tip adsorption of a few atomic layers of H_2O or O_2 is damaging. Region II fatigue crack growth rates accelerate rapidly as H_2O or O_2 pressure is increased from an inert level (1×10^{-2} Pa) to a critical pressure near 10^{-1} Pa. This critical pressure corresponds to a maximum (or inflection in 24 °C water vapor) in the da/dN versus log pressure results shown in Figures 7 and 8. Based on a crack-tip surface adsorption model, a critical

pressure of 1 x 10^{-1} Pa (T = 24 °C, f = 5 Hz) approximates a monolayer of adsorbed H_2O or O_2 [20, 21, 9]. The determination of a critical pressure is based on the formation of fresh titanium surfaces at a rate corresponding to the maximum fatigue crack growth rate observed in Region II. The total pressure of gas required to form an adsorbed monolayer is then calculated by determining the total number of molecules of H_2O or O_2 needed to adsorb on the newly formed surfaces while also taking into consideration the rate of transport of each specie to the tip of the growing fatigue crack [21, 22]. The details of this analysis are shown in Appendix A. Table III compares the pressures corresponding to a maximum fatigue crack growth rate in Region II and the pressure corresponding to an adsorbed monolayer for the test conditions presented. Although further research is required, the correlation of accelerated da/dN in H_2O and O_2 for Region II pressures to monolayer adsorption suggests a crack-tip adsorption damage mechanism. Presumably, the adsorbed water vapor or oxygen lowers the cohesive energy between metallic atoms at a crack tip, resulting in accelerated fatigue crack growth rates [23, 24]. Other mechanisms, such as hydrogen embrittlement, could be argued for water vapor, but are not operative in high purity oxygen. Residual gas analysis of high purity oxygen tests (Table II) indicate that contaminant levels of H_2O are too low to contribute to accelerated da/dN.

The complex fatigue crack growth behavior observed in Region III (H_2O and O_2 pressures greater than $l0^{-1}$ Pa in Figures 7 through 10) may suggest the interaction of multiple crack-tip effects. At Region III water vapor pressures, hydrogen embrittlement is likely to be a significant damage mechanism [6]. Here, a sufficient amount of water vapor can be dissociated at reactive crack-tip surfaces resulting in increased concentrations of atomic hydrogen. Hydrogen can be adsorbed at the reactive crack tip and subsequently absorbed into the crack-tip process zone [25]. Absorbed atomic hydrogen is thought to readily embrittle titanium alloys [26]. However, different Region III fatigue crack growth behaviors are observed in water vapor at 24 °C and 177 °C (increased fatigue crack growth rates are observed at 24 °C and decreased da/dN is observed at 177 °C). XPS analysis of Ti 6-2-2-2-2 samples fatigued in 67 Pa high purity water vapor show that a hydroxide-based film is formed at 24 °C and an oxide/hydroxide film is produced at 177 °C (Figure 11). This observation is consistent with results presented elsewhere for the exposure of several metal films to water vapor at various temperatures [11, 12]. The XPS results suggest that decreased fatigue crack growth rates in water vapor at 177 °C compared to 24 °C da/dN may result from increased levels of a protective surface oxide that limits hydrogen embrittlement [27, 28], presumably by limiting hydrogen entry into the crack-tip process zone. The elevated temperature da/dN decreased until sufficient crack-tip water vapor (greater than approximately 4 Pa in Figure 7) was available; here, ample hydrogen is produced at the crack tip to limit the beneficial effects of the oxide film. With further increases in H_2O pressure (H_2O pressures ranging to 600 Pa), increased levels of crack-tip hydrogen result in a small increase in the fatigue crack growth rate. At room temperature, the hydrogenated film leads to increased levels of crack-tip hydrogen; here, room temperature da/dN is accelerated compared to the fatigue crack growth rates at 177 °C. The Region III behavior in high purity oxygen is difficult to rationalize. An oxide layer is thought to be damaging; researchers have shown that crack-tip surface films limit reversible slip [29, 30]. For oxygen pressures greater than approximately 10 Pa, fatigue crack growth rates are accelerated compared to inert environments suggesting that the formation of an oxide layer is damaging. However, da/dN is shown to decrease with increasing pressure at the beginning of Region III (See Figures 8 through 10). The decrease in da/dN indicates a transition from the Region II behavior, where accelerated fatigue crack growth by adsorption is proposed, to Region III, where irreversible slip is proposed. While both of these mechanisms can lead to accelerated fatigue crack growth rates compared to UHV rates, the formation of an oxide layer at the fatigue crack tip would appear to be less damaging than the adsorption of oxygen. The absorption of oxygen into titanium alloys via the dissolution of a surface oxide has been shown to affect mechanical behavior [31, 32]; however, at the relatively low temperatures used in this study it is not believed that this process has affected the measured fatigue crack growth rates.

Concluding Remarks

Oxygen and water vapor are the damaging species contained in air, and nitrogen does not directly affect the fatigue crack growth behavior of Ti 6-2-2-2-2. The complex behavior of fatigue crack growth rate as a function of O_2 and H_2O pressure suggests that several crack-tip damage processes are operative. Three distinct regions are identified: (1) an inert Region I at low pressures, (2) an adsorption dominated Region II, and 3) Region III where the behavior is affected by both an oxide and hydrogen embrittlement. In Region II, where monolayer adsorption of O_2 and H_2O is predicted (See Appendix A), accelerated fatigue crack growth may result from an adsorption process that reduces the energy of metal-metal bonds at the crack-tip. For Region III, O_2 and H_2O results suggest that fatigue crack growth is dominated by the formation of complex crack-tip films. In high purity O_2 (24 °C and 177 °C) and H_2O (177 °C), similar fatigue crack growth behavior and XPS results suggest that crack-tip oxide-based films dominate crack growth behavior. Here, an oxide film is thought to be damaging by inhibiting reversible slip. At room temperature in Region III, H_2O exposure produces a hydroxide-based crack-tip film and fatigue crack growth rates that are accelerated compared to O_2 (24 °C and 177 °C) and H_2O (177 °C) environments. It is speculated that at room temperature a hydroxide-based film allows for greater hydrogen uptake by the crack-tip process zone than is possible at elevated temperature where an oxide-based film can readily form on crack surfaces.

References

1. Wei, R.P.; Pao, P.S.; Hart, R.G.; Weir, T.W.; and Simmons, G.W.: Fracture Mechanics and Surface Chemistry Studies of Fatigue Crack Growth in an Aluminum Alloy. *Metallurgical Transactions A*, 11A, 1980, pp. 151-158.

2. Gough, H.J.; and Sopwith, D.G.: Atmospheric Action as a Factor in Fatigue of Metals. J *Inst. Metals*, 49, 1932, pp. 93-122.

3. Grinberg, N.M.: The Effect of Vacuum on Fatigue Crack Growth. *Int. J Fatigue*, April 1982, pp. 83-95.

4. Wadsworth, N.J.; and Hutchings, J.: The Effect of Atmospheric Corrosion on Metal Fatigue. *Phil. Mag.*, Series 8, 3 (34), 1958, pp. 1154-1166.

5. Meyn, D.A.: An Analysis of Frequency and Amplitude Effects on Corrosion Fatigue Crack Propagation in Ti-8Al-1Mo-1V. *Metallurgical Transactions*, 2, 1971, pp. 853-865.

6. Sarrazin-Baudoux, C.; Lesterlin, S.; and Petit, J.: Atmospheric Influence on Fatigue Crack Propagation in Titanium Alloys at Elevated Temperature. *Elevated Temperature Effects on Fatigue and Fracture, ASTM STP 1297*, 1997, pp. 117-139.

7. Piascik, R. S.; and Newman, J.C., Jr.: An Extended Compact Tension Specimen for Fatigue Crack Growth and Fracture Testing. *Int. Journ. of Fracture*, 76, 1995, pp. R43-R48.

8. ASTM: Standard Test Method for Measurement of Fatigue Crack Growth Rates. *Annual Book of ASTM Standards, E 647-99*, 03.01, 2000, pp. 591-630.

9. Elber, W.: The Significance of Fatigue Crack Closure. *Damage Tolerance in Aircraft Structures, ASTM STP 486*, 1971, pp. 230-242.

10. Feldman, L.C.; and Mayer, J.W.: *Fundamentals of Surface and Thin Film Analysis.* North-Holland, 1986, pp. 213-231.

11. Fuggle, J.C.; Watson, L.M.; Fabian, D.J.; and Affrossman, S.: X-Ray Photoelectron Studies of the Reaction of Clean Metals (Mg, Al, Cr, Mn) with Oxygen and Water Vapor. *Surface Science,* 49, 1975, pp. 61-76.

12. Padalia, B.D.; Gimzewski, J.K.; Affrossman, S.; Lang, W.C.; Watson, L.M.; and Fabian, D.J.: The Reactions of Oxygen and Water with the Rare-Earth Metals Terbium to Lutetium Studied by X-Ray Photoelectron Spectroscopy. *Surface Science,* 61, 1976, pp. 468-482.

13. Broek, D.: *Elementary Engineering Fracture Mechanics,* 4th ed., Martinum Nijhoff, Dordrecht, Netherlands, 1986, pp. 321-323.

14. Christensen, R.H.: Fatigue Crack Growth Affected by Metal Fragments Wedged Between Opening-Closing Crack Surfaces. *Applied Materials Research,* October 1963, pp. 207-210.

15. Suresh, S.; Zamiski, G.F.; and Ritchie, R.O.: Oxide-Induced Crack Closure: An Explanation for Near-Threshold Corrosion Fatigue Crack Growth Behavior. *Metallurgical Transactions A,* Vol. 12A, 1981, pp. 1435-1443.

16. Suresh, S.; and Ritchie, R.O.: Some Considerations on the Modeling of Oxide-Induced Fatigue Crack Closure Using Solutions for a Rigid Wedge Inside a Linear Elastic Crack. *Scripta Metallurgica,* Vol. 17, 1983, pp. 575-580.

17. McClung, R.C.: The Influence of Applied Stress, Crack Length, and Stress Intensity Factor on Crack Closure. *Metallurgical Transactions A,* 22A, 1991, pp. 1559-1571.

18. Newman, J.A.: *The Effects of Load Ratio on Threshold Fatigue Crack Growth of Aluminum Alloys,* PhD dissertation, Virginia Tech, October, 2000.

19. Smith, S.W.; and Piascik, R.S.: An Indirect Technique for Determining Closure-Free Fatigue Crack Growth Behavior. *Fatigue Crack Growth Thresholds, Endurance Limits, and Design, ASTM STP 1372,* J.C. Newman, Jr. and R.S. Piascik, eds., 1999, pp. 109-122.

20. Snowden, K.U.: The Effect of Atmosphere on the Fatigue of Lead. *Acta Metallurgica,* Vol. 12, 1964, pp. 295-303.

21. Bradshaw, F.J.: The Effect of Gaseous Environment on Fatigue Crack Propagation. *Scripta Metallurgica, Vol.* 1, 1967, pp. 41-43.

22. Hénaff, G.; Marchal, K.; and Petit, J.: On Fatigue Crack Propagation Enhancement by a Gaseous Atmosphere: Experimental and Theoretical Aspects. *Acta Metallurgica,* 43 (8), 1995, pp. 2931-2942.

23. Fuller, E.R., Jr.; Lawn, B.R.; and Thomson, R.M.: Atomic Modeling of Chemical Interactions at Crack Tips. *Acta Metallurgica,* 28, 1980, pp. 1407- 1414.

24. Petch, N.J.: The Lowering of Fracture-Stress due to Surface Adsorption. *Phil Mag.* Ser. 8, 1, 1956, pp. 331-337.

25. Tien, J.K.; Richards, R.J.; Buck, O.; and Marcus, L.: Model of Dislocation Sweep-In of Hydrogen During Fatigue Crack Growth. *Scripta Metallurgica,* Vol. 9, 1975, pp. 1097-1101.

26. Pao, P.S.; and Wei, R.P.: Hydrogen-Enhanced Fatigue Crack Growth in Ti-6Al-2Sn-4Zr-2Mo-0.1Si. *Titanium: Science and Technology, Proceedings of the Fifth International Conference on Titanium*, Vol. 4, Deutsche Gesellschaft Fur Metallkunde E.V., 1985, pp. 2503-2510.

27. DeLuccia, J.J.: *Electrolytic Hydrogen in Beta Titanium*, NADC-76207-30, Naval Air Development Center, Warminster, PA, 1976.

28. Schutz, R.W.; and Covington, L.C.: Effect of Oxide Films on the Corrosion Resistance of Titanium. *Corrosion, 37* (10), 1981, pp. 585-591.

29. Roscoe, R.: Strength of Metal Single Crystals. *Nature*, 133, 1934, p. 912

30. Sieradzki, K.: The Effect of Thin Film Formation at Crack Tips on Fracture. *Acta Metallurgica*, 30, 1982, pp. 973 -982.

31. Wallace, T.A.; Wiedemann, K.E.; and Clark, R.K.: Oxidation Characteristics of Beta-21S in Air in the Temperature Range 600 to 800°C. *Titanium '92: Science and Technology*, F. H. Froes and I. Caplan, eds., TMS, 1993, pp. 2177-2184.

32. Wallace, T.A.: The Effect of Oxidation Exposure on the Mechanical Properties of Timetal-1100 (Ti-6Al-2.75Sn-4Zr-0.4Mo-0.07O_2-0.02Fe wt.%). *Titanium '95: Science and Technology*, P.A. Blenkinsop, W.J. Evans, and P.A. Flower, eds., The Institute of Materials, 1996, pp. 1943-1950.

33. Harra, D.J.: Review of Sticking Coefficients and Sorption Capacities of Gases on Titanium Films. J *Vac. Sci. Technol.*, Vol. 13, No. 1, Jan/Feb 1976, pp. 471-474.

34. O'Hanlon, J.F.: *A User's Guide to Vacuum Technology.* Second ed., John Wiley and Sons, 1989, pp. 9-10, 435.

35. Ogawa, T.; Tokaji, K.; and Ohya, K.: The Effect of Microstructure and Fracture Surface Roughness on Fatigue Crack Propagation in a Ti-6Al-4V Alloy. *Fatigue Fract. Engng. Mater. Struct.*, Vol. 16, No. 9, 1993, pp. 973-982.

Appendix A: Determination of critical pressures for the adsorption of one monolayer of oxygen or water vapor on clean titanium fatigue surfaces.

Snowden [20] determined a critical pressure required to have one monolayer adsorb on to newly created fatigue surface during one fatigue cycle. Later Bradshaw [21] also modeled this problem accounting for the impedance of a fatigue crack for the flow of gaseous specie from an exterior environment to the tip of a fatigue crack. Hénaff et al. [22] modified the impedance equations. The approach used herein takes into consideration each of these works.

For the adsorption regime being analyzed, the pressures used are relatively low. Therefore, it will be assumed that molecular flow is present and the ideal gas law can be applied.

$$\left(P_o - P_1\right) \times \dot{V} = \frac{\dot{n}}{\text{Prob}} \times k \times T \qquad \text{(A-1)}$$

Where: P_0, P_1 are the pressures of the test environment and at the crack tip, respectively; $\dot{V}$ is the volumetric flow rate of gas to the crack tip; $\dot{n}$ and Prob are the adsorption rate and sticking probability of gaseous species on newly formed crack surfaces; k is Boltzmann's constant and T is temperature. Values for sticking probability are supplied in Table A-I. These values are evaluated using a linear regression for the data supplied in Harra for the adsorption of oxygen and water vapor on a continuously deposited titanium film [33].

Table A-I. Sticking probability for oxygen and water vapor on a titanium film.

Environment	Prob	
	at 24°C	at 177°C
O_2	0.8	0.73
H_2O	0.66	0.49

The volumetric flow rate of gas to the crack tip can be determined by adapting the work of Hénaff et al. [22].

$$\dot{V} = \frac{4}{3}\nu\frac{t\alpha^2}{4}\left[\ln\left(\frac{\delta(t/2)}{\delta(\Delta a)}\right) - \beta\left(\frac{1}{\delta(\Delta a)} - \frac{1}{\delta(t/2)}\right)\right]^{-1} \qquad \text{(A-2)}$$

This equation is based on a crack impedance where: ν is the average gas velocity; t is the specimen thickness and $\delta(x)$ is the crack tip opening at a distance x from the crack tip. α is defined as:

$$\alpha = \sqrt{\frac{2}{\pi}} \frac{K_{mean}}{E} \qquad \text{(A-3)}$$

Where: K_{mean} is the mean stress-intensity factor and E is the elastic modulus ($\approx 120 \times 10^3$ MPa for Ti 6-2-2-2-2). Therefore, α is approximately equal to 6.58×10^{-5} $m^{1/2}$ for Ti 6-2-2-2-2 at $\Delta K = 6.6$ MPa$\sqrt{m}$ and R = 0.5. As previously stated, molecular flow is being assumed; therefore:

$$v(m/\sec) = \left(\frac{8 \times k \times T}{\pi \times M} \right)^{1/2} \qquad \text{from [34]} \qquad \text{(A-4)}$$

Where: M is the molecular weight of the gaseous specie being examined. Table A-II provides values of average gas velocity for oxygen and water vapor using equation A-4.

Table A-II. Average gas velocity for oxygen and water vapor in the crack tip region.

Environment	ν (m/sec)	
	at 24°C	at 177°C
O_2	443.3	545.7
H_2O	590.7	727.1

Two specific lengths (t/2, Δa) are used in equation A-2 for the determination of crack tip opening values. These limits are shown in Figure A1. The shaded region in Figure A-1 depicts a control volume for the increment of crack growth Δa, the crack growth increment for one fatigue cycle. This control volume contains the gaseous species available for adsorption onto the surfaces created during fatigue crack propagation. The gaseous species available for adsorption enters the crack from the area t/2 x δ(t/2). t/2 is half the specimen thickness or the maximum diffusion distance for a molecule entering the crack region. Crack tip opening can be calculated using:

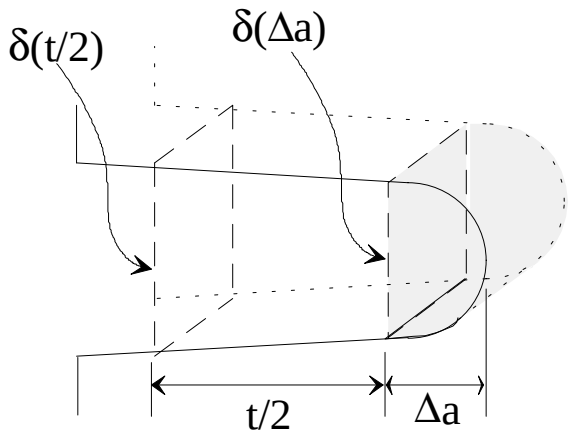

Figure A-1. Crack tip geometry used for gaseous impedance calculations.

$$\delta(x) = \alpha\sqrt{x} + \beta \qquad \text{(A-5)}$$

Where: $\beta = \frac{K_{av}^2}{4E\sigma_o}$. σ_o is the flow stress for the material being tested (σ_o is approximately equal to 1140 MPa for Ti 6-2-2-2-2).

The rate of adsorption can be represented by:

$$\dot{n} = \left(\frac{da}{dN} \times f\right) \times 2 \times \left(\frac{t}{2}\right) \times r \times \text{coverage} \qquad \text{(A-6)}$$

Where: da/dN is the maximum fatigue crack growth rate in the adsorption regime; *f* is frequency; r is surface roughness and coverage is the molecular coverage of adsorbed species on the crack tip. Ogawa et al. [35] measured surface roughness values between 1 and 2 for Ti 6Al-4V. A value of approximately 1.3 was obtained at a fatigue crack growth rate of 1×10^{-8} m/cycle. This value will be used for the calculations presented in the work. Harra [33] has reported a molecular coverage of 2.4×10^{20} molecules/m^2 for oxygen on titanium and 3.0×10^{20} molecules/m^2 for H_2O on titanium. The term $\left(\frac{da}{dN} \times f\right)$, in equation A-6, must be multiplied by 2 to account for the top and bottom fatigue surfaces. t is divided by 2, in equation A-6, to model only half of the specimen thickness since gaseous species can enter the crack tip region from either face of the sheet specimen.

P_{crit} can be solved for a known da/dN, *f* and T in high purity O_2 or H_2O with the information provided above. Critical pressures for the adsorption of 1 monolayer of oxygen or water vapor for the loading conditions examined are provided in Table III.

Table I. Results of partial pressure analyses determined by QMS measurements during high purity water vapor tests.

Total Pressure (Pa)	PP (H_2O) (Pa)	PP (O_2) (Pa)	PP (N_2 + CO) (Pa)	PP (H_2) (Pa)	PP (CO_2) (Pa)	PP (Methanol) (Pa)
UHV 1.15×10^{-7}	3.47×10^{-9}	$< 1 \times 10^{-9}$	1.83×10^{-8}	9.24×10^{-8}	$< 1 \times 10^{-9}$	$< 1 \times 10^{-9}$
1.87×10^{-4}	1.58×10^{-4}	2.88×10^{-7}	9.06×10^{-7}	2.69×10^{-5}	7.17×10^{-7}	5.91×10^{-7}
2.00×10^{-3}	1.82×10^{-3}	1.03×10^{-6}	4.03×10^{-6}	1.74×10^{-4}	1.92×10^{-6}	9.29×10^{-6}
1.47×10^{-2}	1.36×10^{-2}	6.35×10^{-5}	2.04×10^{-4}	3.52×10^{-4}	4.16×10^{-4}	9.77×10^{-5}
2.67×10^{-1}	2.56×10^{-1}	3.86×10^{-3}	1.15×10^{-3}	1.84×10^{-3}	2.34×10^{-3}	1.13×10^{-3}
2.93	2.85	1.59×10^{-2}	9.45×10^{-3}	1.83×10^{-2}	2.04×10^{-2}	1.55×10^{-2}
34.3	33.3	3.96×10^{-1}	9.30×10^{-2}	2.47×10^{-1}	1.45×10^{-1}	1.13×10^{-1}
207	202	1.43	4.90×10^{-1}	1.25	1.16	3.63×10^{-1}

Table II. Results of partial pressure analyses determined by QMS measurements during high purity oxygen tests.

Total Pressure (Pa)	PP (O_2) (Pa)	PP (H_2O) (Pa)	PP (N_2 + CO) (Pa)	PP (H_2) (Pa)	PP (CO_2) (Pa)	PP (Methanol) (Pa)
UHV 1.15×10^{-7}	$< 1 \times 10^{-9}$	3.47×10^{-9}	1.83×10^{-8}	9.24×10^{-8}	$< 1 \times 10^{-9}$	$< 1 \times 10^{-9}$
1.07×10^{-4}	8.95×10^{-5}	1.15×10^{-5}	2.31×10^{-6}	2.32×10^{-6}	1.06×10^{-6}	$< 1 \times 10^{-9}$
1.19×10^{-3}	1.13×10^{-3}	1.29×10^{-5}	2.55×10^{-6}	4.47×10^{-5}	1.56×10^{-6}	2.93×10^{-6}
1.25×10^{-2}	1.23×10^{-2}	2.80×10^{-5}	8.69×10^{-6}	1.86×10^{-4}	7.49×10^{-6}	3.29×10^{-5}
1.33×10^{-1}	1.32×10^{-1}	3.38×10^{-4}	2.16×10^{-4}	3.17×10^{-5}	6.48×10^{-5}	2.95×10^{-4}
2.27	2.26	2.07×10^{-3}	1.42×10^{-3}	5.09×10^{-5}	2.02×10^{-3}	4.21×10^{-3}
18.9	18.8	1.29×10^{-2}	9.26×10^{-3}	9.02×10^{-4}	1.70×10^{-2}	3.42×10^{-2}
206	205	1.27×10^{-1}	1.20×10^{-1}	4.48×10^{-3}	1.81×10^{-1}	4.16×10^{-1}

Table III. Comparison of Region II observed P_{crit} and the pressure calculated to adsorb a monolayer (P_{mono}) of O_2 or H_2O at T = 24 °C, 177 °C, f = 5 Hz, f = 0.5 Hz.

Environment	Temp. (°C)	frequency (Hz)	da/dN_{max} (m/cycle)	P_{crit} (Pa) observed	P_{mono} (Pa) calculated
oxygen	24	5	1.27×10^{-8}	0.13	0.18
oxygen	177	5	1.55×10^{-8}	0.27 - 1.3	0.30
oxygen	24	0.5	2.25×10^{-8}	0.025 - 0.47	0.033
oxygen	177	0.5	2.04×10^{-8}	0.099	0.040
water vapor	24	5	1.52×10^{-8} *	0.18 *	0.25
water vapor	177	5	1.81×10^{-8}	0.17	0.50

* - Inflection point in da/dN versus log (P) data used.

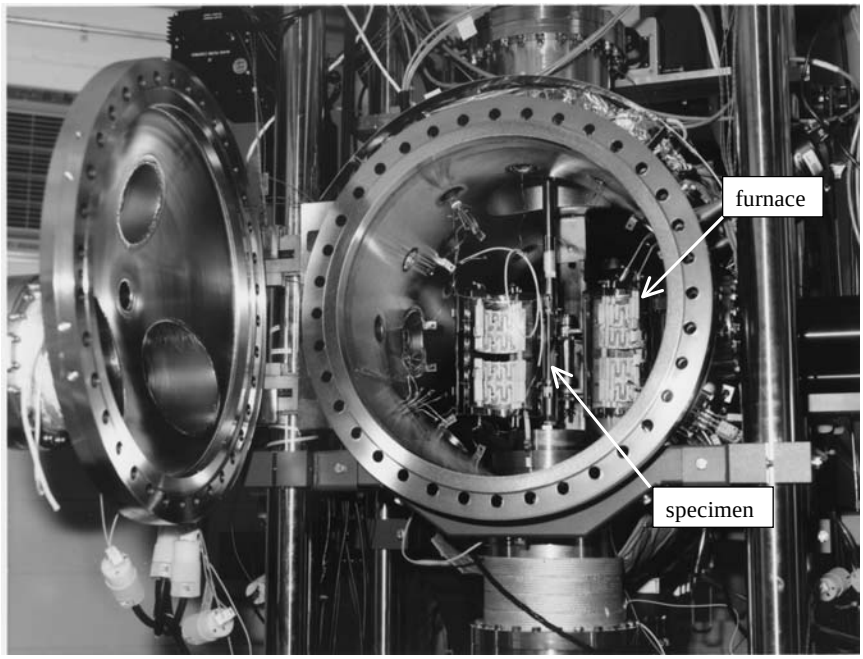

Figure 1a. Front view of vacuum chamber used for controlled environment tests. Front door is open to show specimen mounting and the furnace used for 177 °C tests.

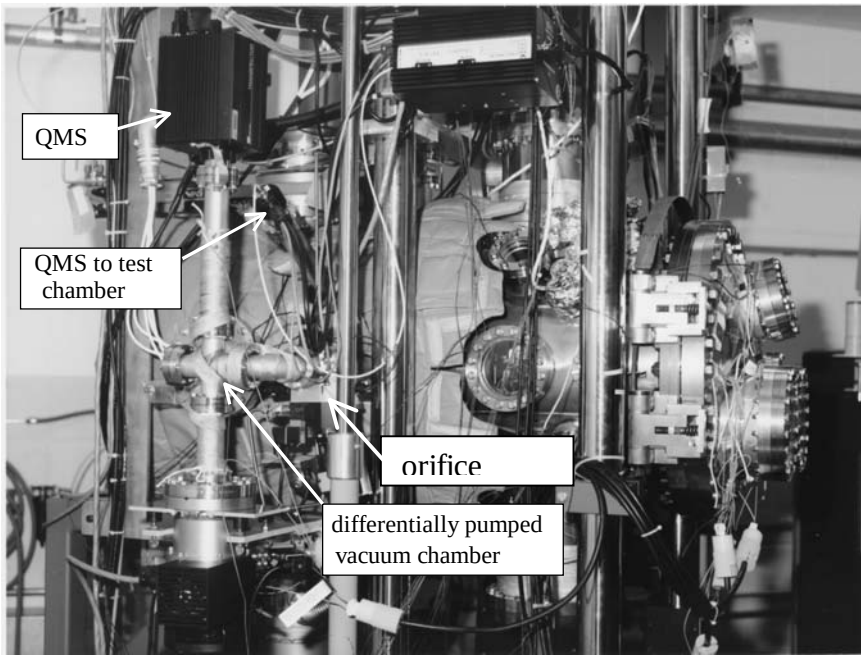

Figure 1b. Side view of vacuum chamber used for controlled environment tests. Differentially pumped vacuum chamber and both QMS's are indicated.

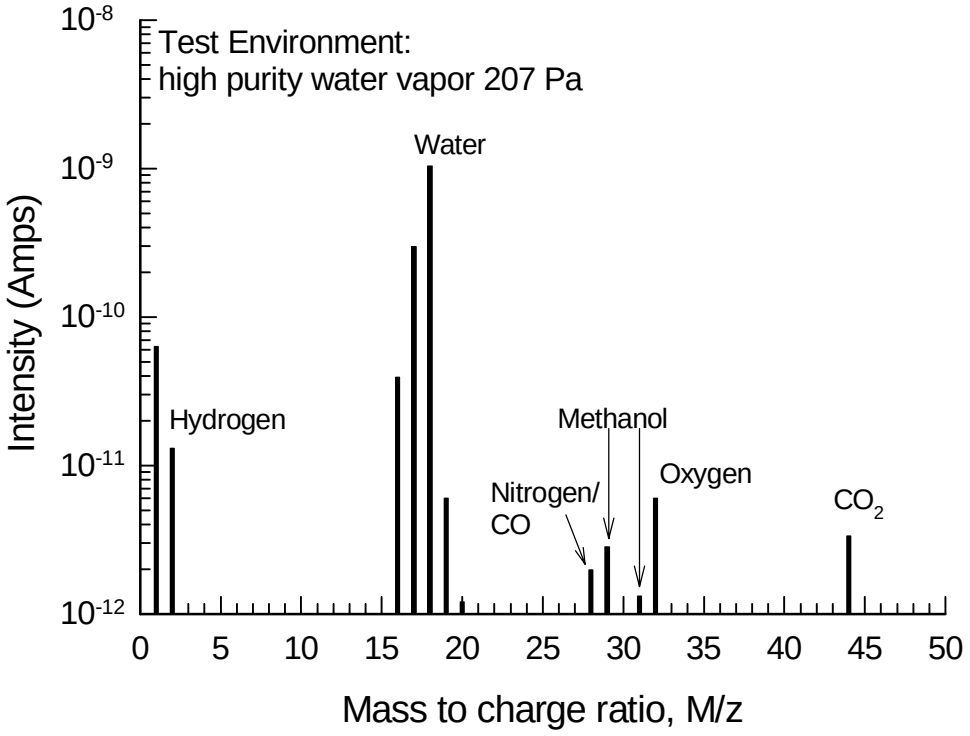

Figure 2. Residual gas analysis results for mass to charge ratios of 0 to 50 for a high purity water vapor test at 207 Pa. The molecules responsible for selected peaks are identified.

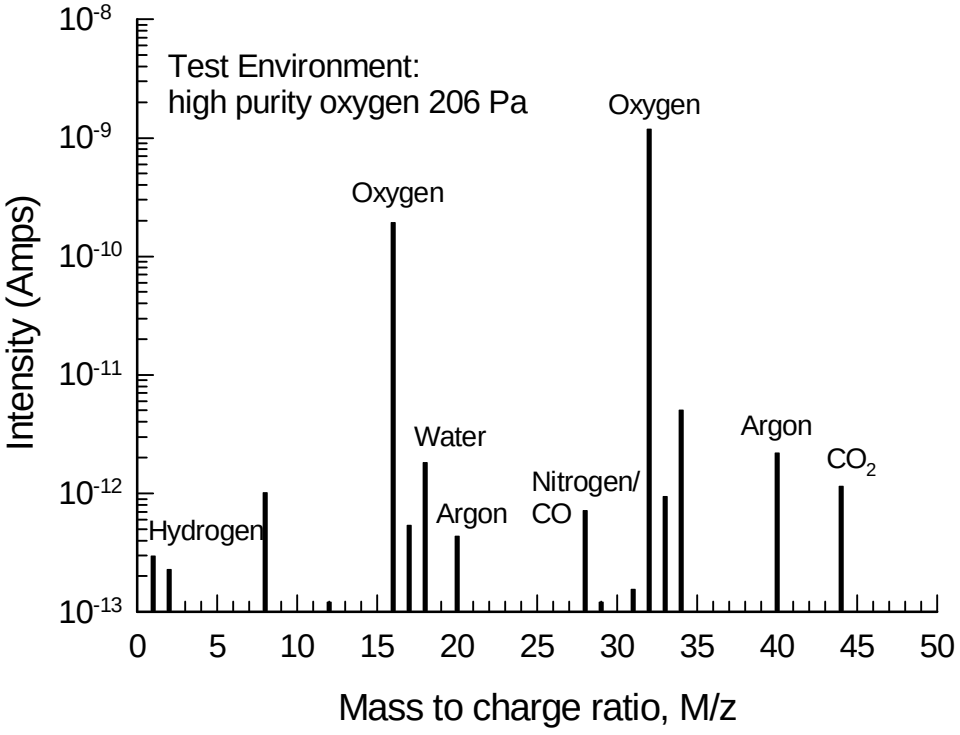

Figure 3. Residual gas analysis results for mass to charge ratios of 0 to 50 for a high purity oxygen test at 206 Pa. The molecules responsible for selected peaks are identified.

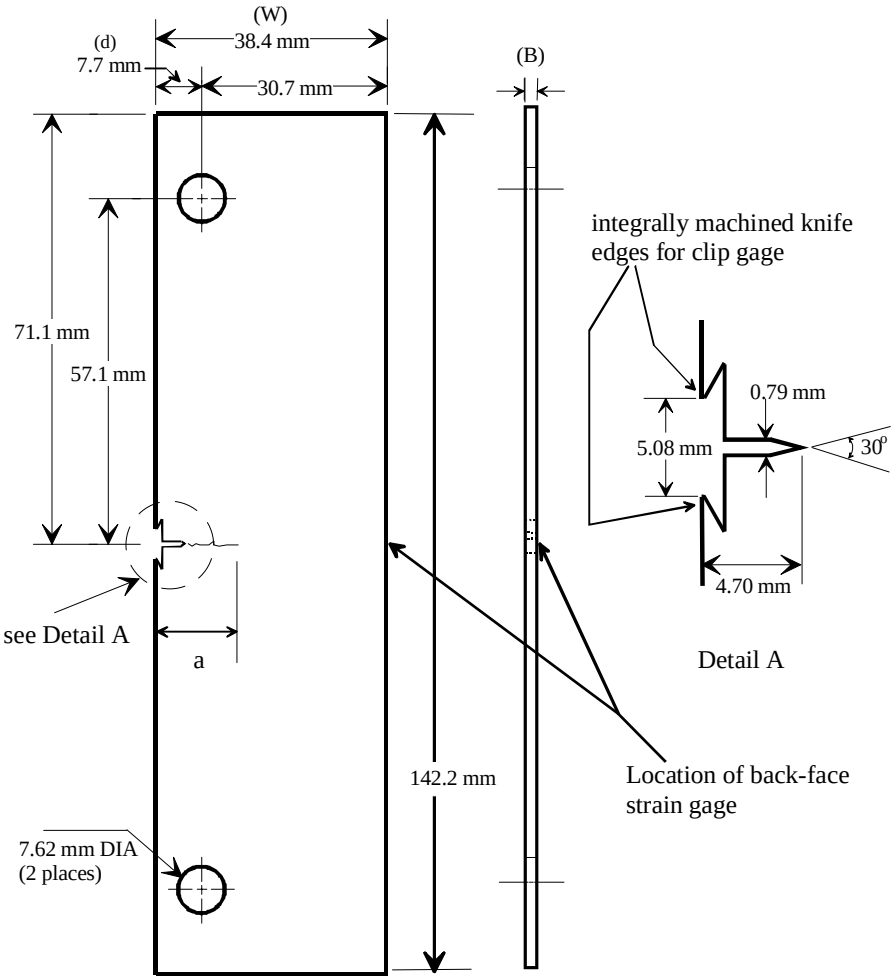

Figure 4. Specimen design for eccentrically-loaded single edge crack tension (ESE(T)) specimen.

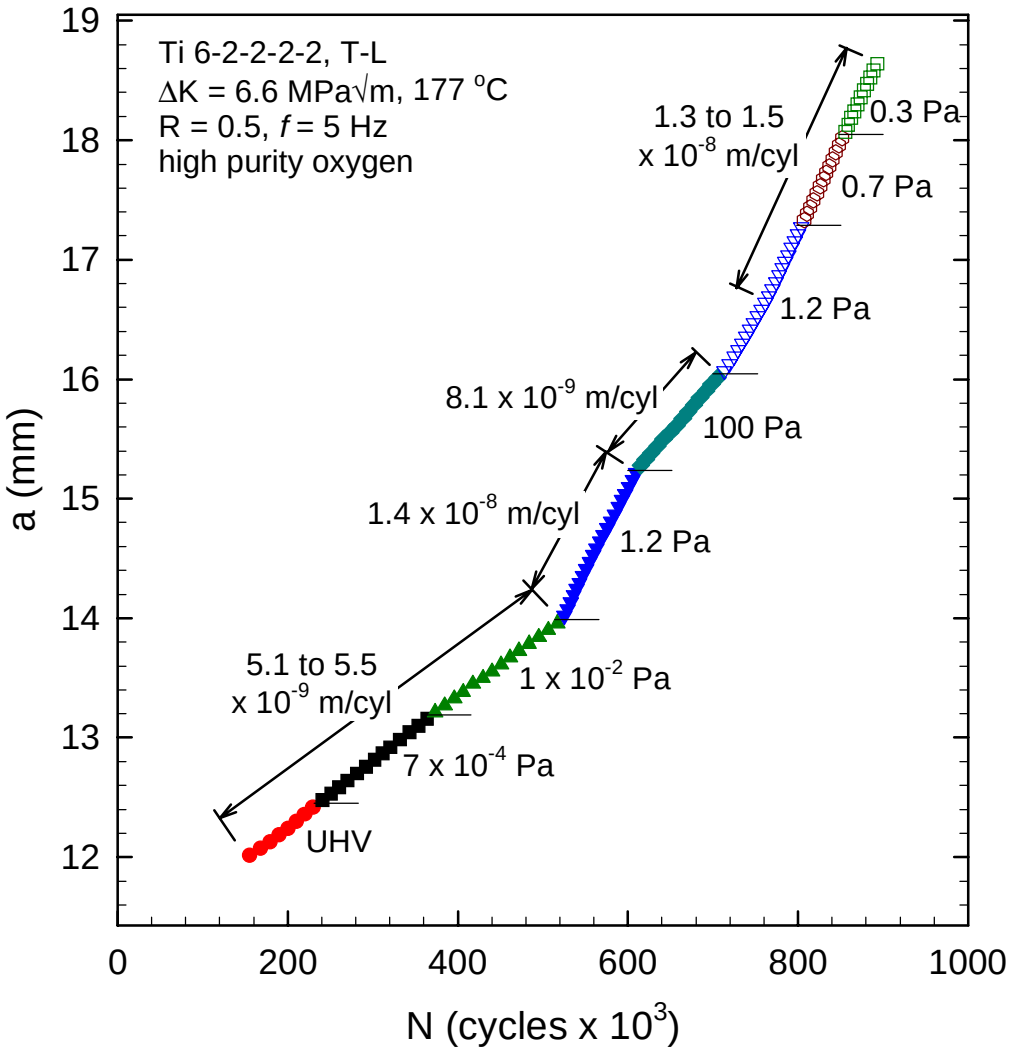

Figure 5. Crack length versus cycle count for high purity oxygen testing. Noted are fatigue crack growth rates for four regions of similar fatigue crack growth rate (linear Δa/ΔN).

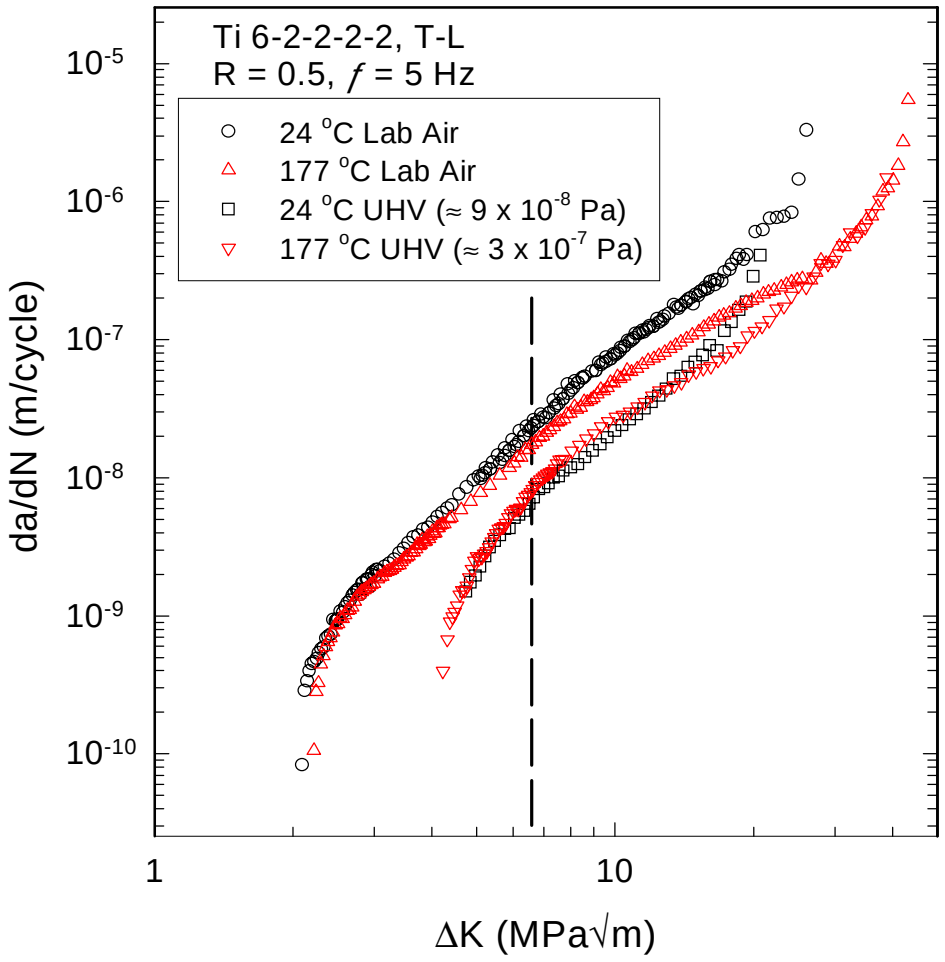

Figure 6. Fatigue crack growth rate versus cyclic stress-intensity for laboratory air and ultrahigh vacuum testing at 24 °C and 177 °C.

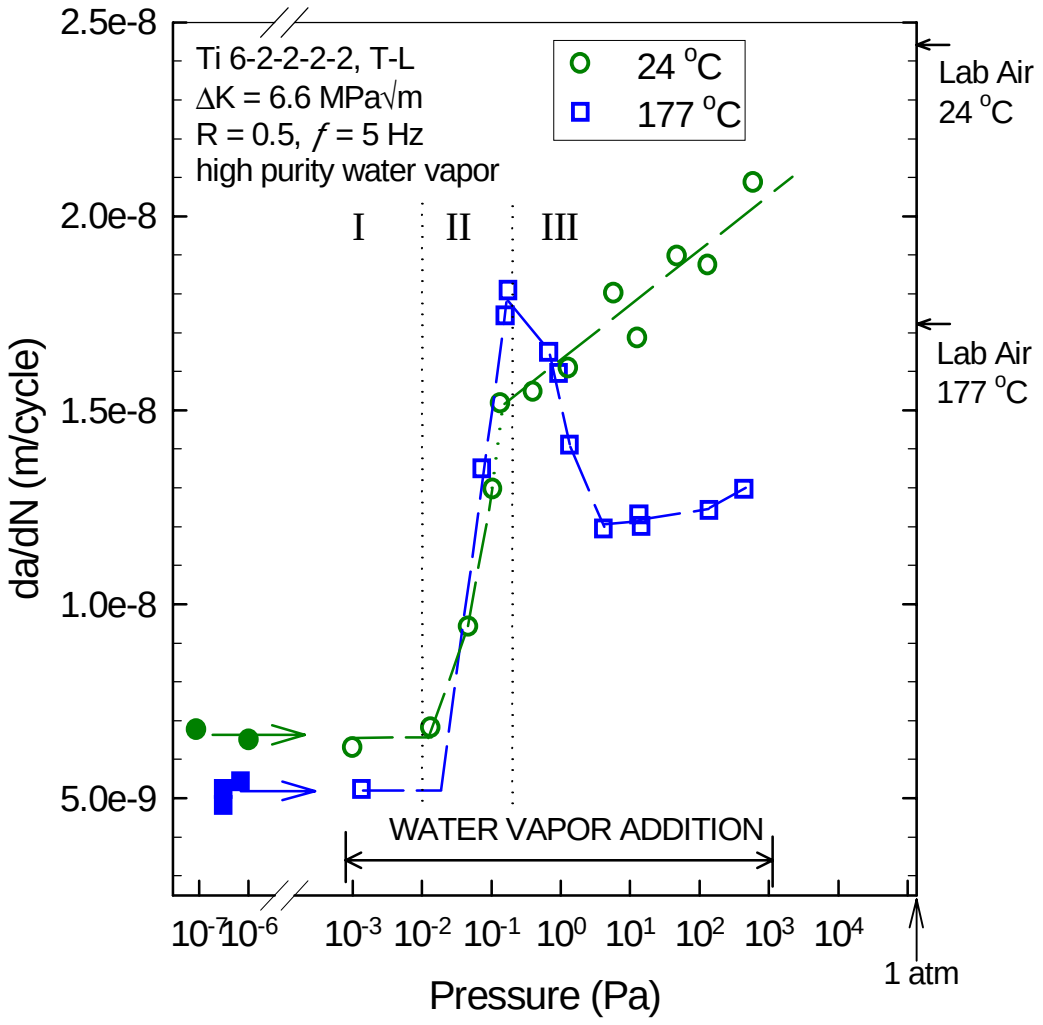

Figure 7. Plot of fatigue crack growth rate versus pressure for tests conducted in high purity water vapor and UHV. Fatigue crack growth rates measured in UHV are represented by closed symbols and open symbols represent data for high purity water vapor test environments. Each data point represents a steady-state crack growth rate at constant ΔK.

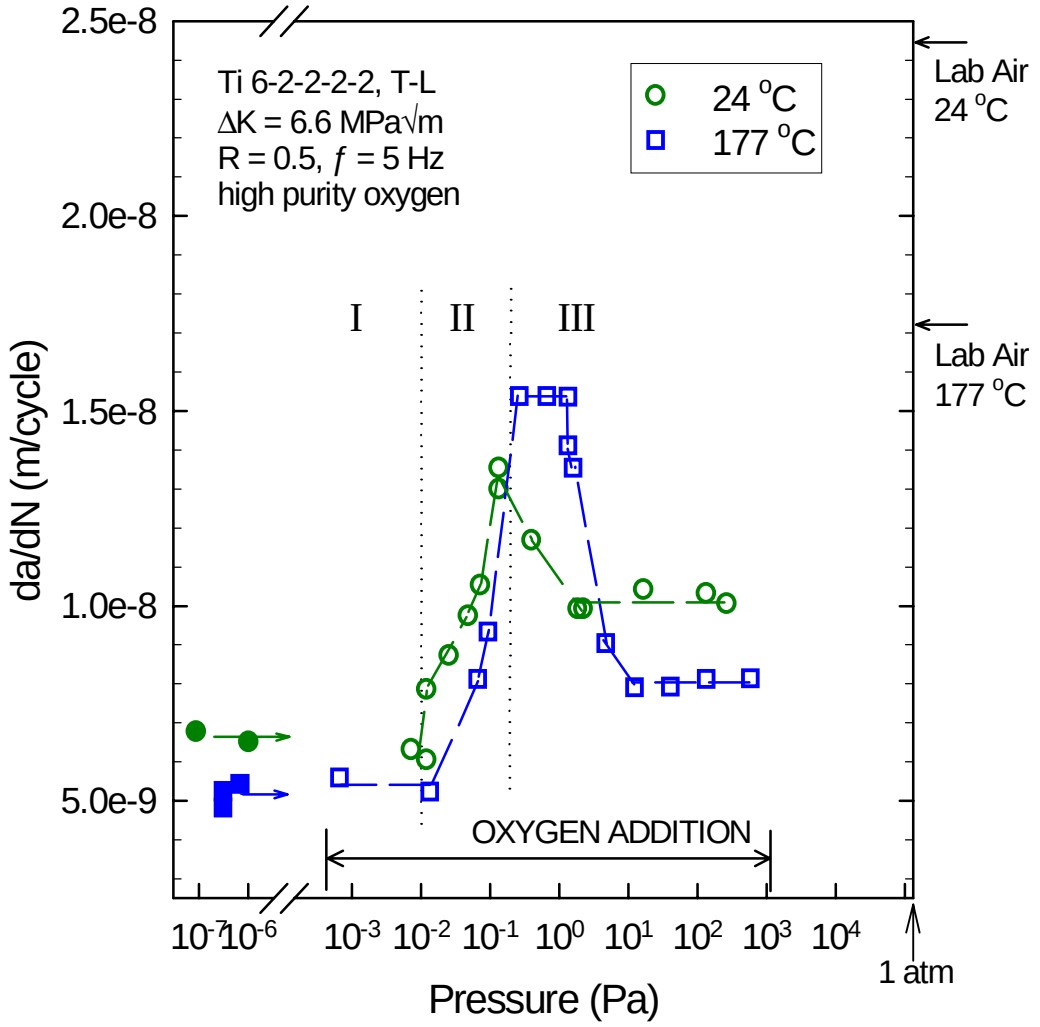

Figure 8. Plot of fatigue crack growth rate versus pressure for tests conducted in high purity oxygen and UHV. Fatigue crack growth rates measured in UHV are represented by closed symbols and open symbols represent data for high purity oxygen test environments. Each data point represents a steady-state crack growth rate at constant ΔK.

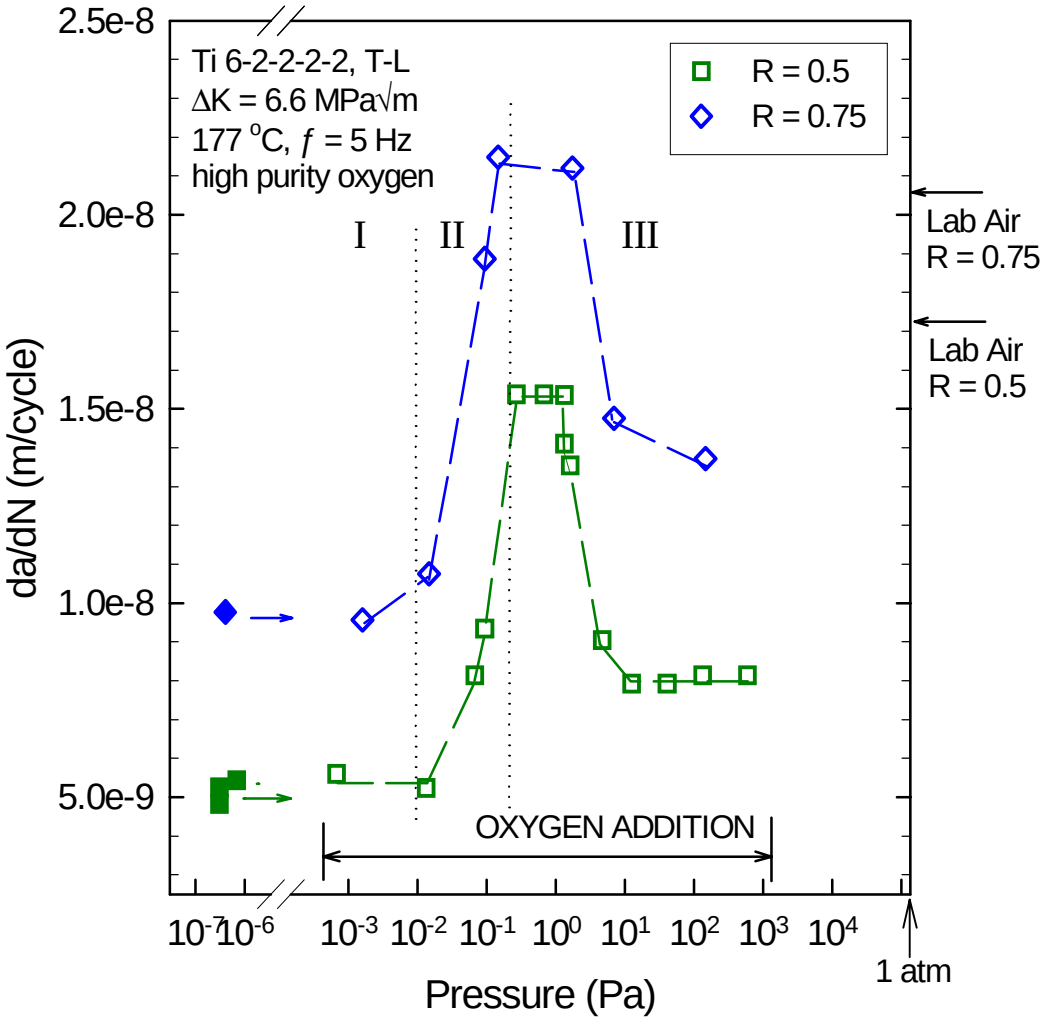

Figure 9. Plot of fatigue crack growth rate versus pressure for tests conducted in high purity oxygen and UHV at ΔK = 6.6 MPa√m, frequency = 5 Hz, and R = 0.5 and 0.75. Fatigue crack growth rates measured in UHV are represented by closed symbols and open symbols represent data for high purity oxygen test environments. Each data point represents a steady-state crack growth rate at constant ΔK.

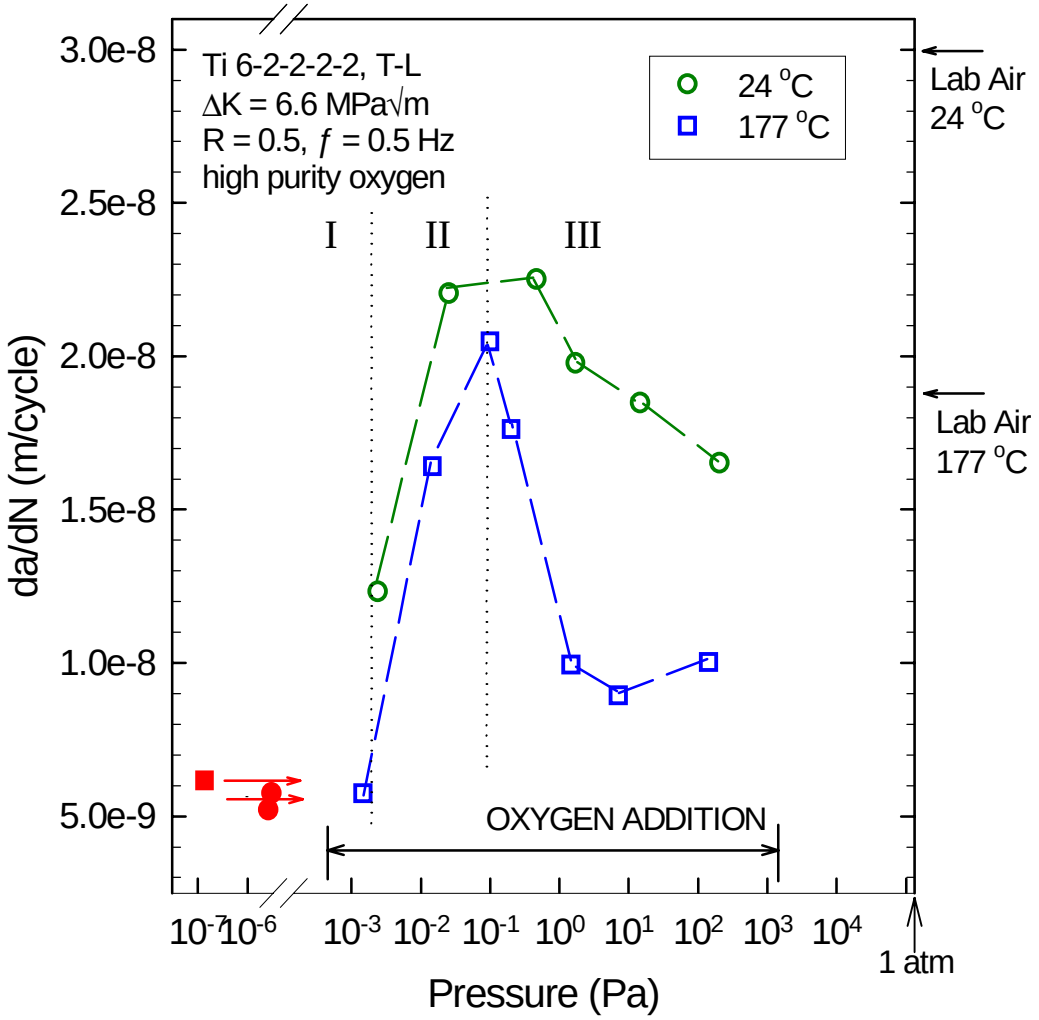

Figure 10. Plot of fatigue crack growth rate versus pressure for tests conducted in high purity oxygen and UHV at ΔK = 6.6 MPa√m, frequency = 0.5 Hz, and R = 0.5. Fatigue crack growth rates measured in UHV are represented by closed symbols and open symbols represent data for high purity oxygen test environments. Each data point represents a steady-state crack growth rate at constant ΔK.

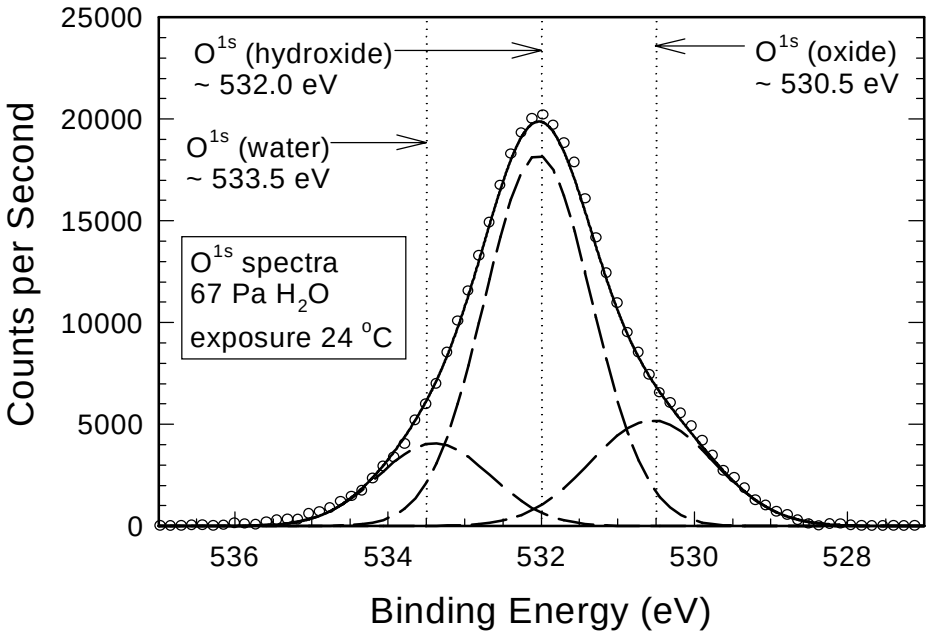

a)

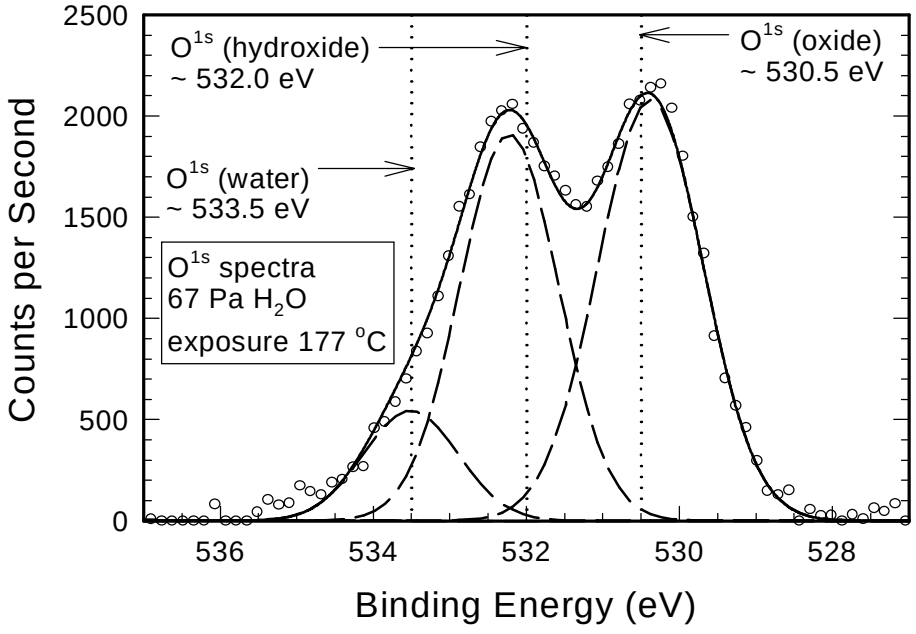

b)

Figure 11. Shown are XPS spectra produced for Ti 6-2-2-2-2 fatigue crack surfaces from specimens tested in 67 Pa water vapor at a) 24 °C and b) 177 °C. Constituent peaks are shown as dashed lines and the binding energy of O^{1s} photoelectrons for three compounds are identified by dotted lines.

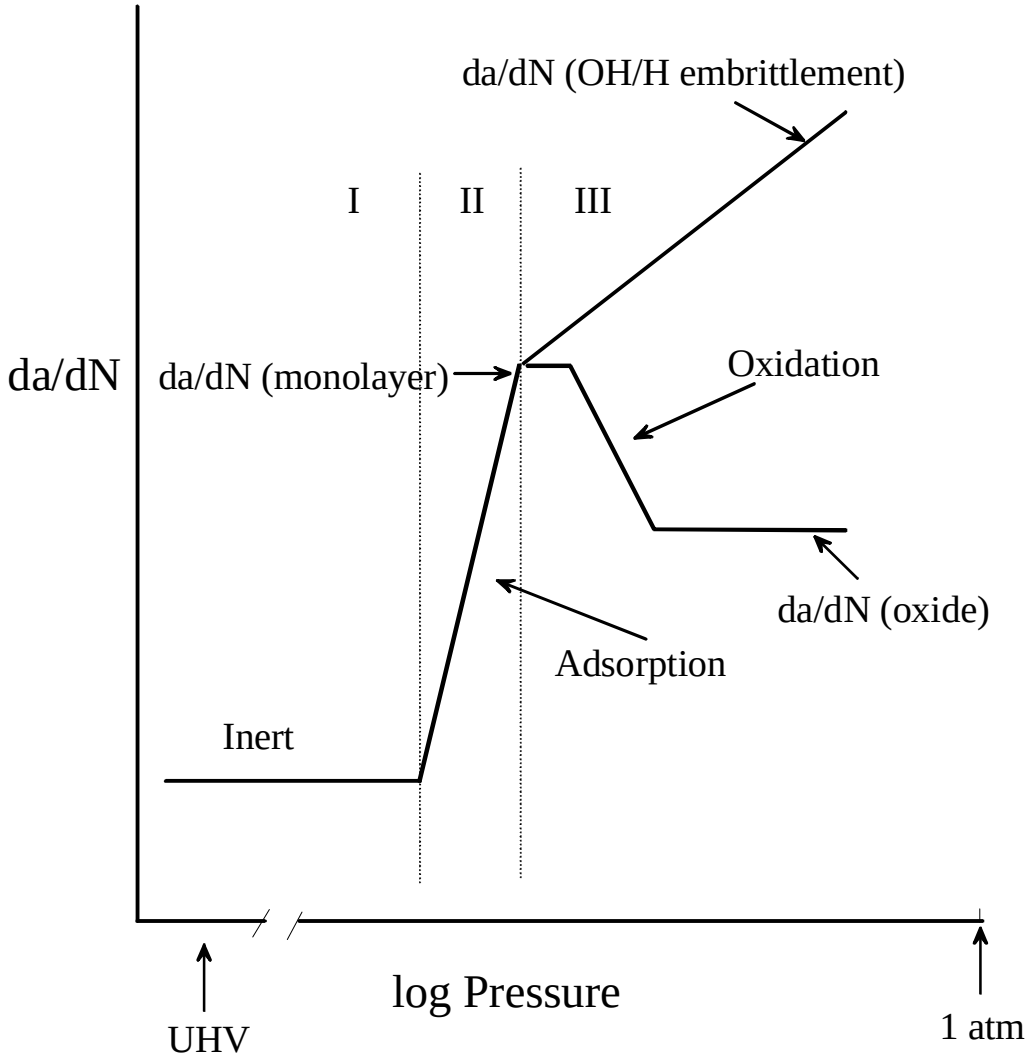

Figure 12. Schematic of the fatigue crack growth behavior observed for Ti 6-2-2-2-2 in high purity water vapor and oxygen at 24 °C and 177 °C.

REPORT DOCUMENTATION PAGE

Form Approved
OMB No. 0704-0188

1. AGENCY USE ONLY (*Leave blank*)	2. REPORT DATE	3. REPORT TYPE AND DATES COVERED
	December 2001	Technical Memorandum

4. TITLE AND SUBTITLE

The Effect of O_2, H_2O, and N_2 on the Fatigue Crack Growth Behavior of an $\alpha+\beta$ Titanium Alloy at 24 °C and 177 °C

5. FUNDING NUMBERS

WU 706-62-31-01

6. AUTHOR(S)

Stephen W. Smith and Robert S. Piascik

7. PERFORMING ORGANIZATION NAME(S) AND ADDRESS(ES)

NASA Langley Research Center
Hampton, VA 23681-2199

8. PERFORMING ORGANIZATION REPORT NUMBER

L-18127

9. SPONSORING/MONITORING AGENCY NAME(S) AND ADDRESS(ES)

National Aeronautics and Space Administration
Washington, DC 20546-0001

10. SPONSORING/MONITORING AGENCY REPORT NUMBER

NASA/TM-2001-211248

11. SUPPLEMENTARY NOTES

12a. DISTRIBUTION/AVAILABILITY STATEMENT

Unclassified-Unlimited
Subject Category 26 Distribution: Standard
Availability: NASA CASI (301) 621-0390

12b. DISTRIBUTION CODE

13. ABSTRACT *(Maximum 200 words)*

To study the effects of atmospheric species on the fatigue crack growth behavior of an $\alpha+\beta$ titanium alloy (Ti 6-2-2-2-2) at room temperature and 177 °C, fatigue tests were performed in laboratory air, ultrahigh vacuum, and high purity water vapor, oxygen, nitrogen and helium at various partial pressures. Accelerated fatigue crack growth rates in laboratory air compared to ultrahigh vacuum are linked to the damaging effects of both water vapor and oxygen. Observations of the fatigue crack growth behavior in ultrahigh purity environments, along with surface film analysis using X-ray photoelectron spectroscopy (XPS), suggest that multiple crack-tip processes govern the damaging effects of air. Three possible mechanisms are proposed: 1) at low pressure ($< 10^{-1}$ Pa), accelerated da/dN is likely due to monolayer adsorption on crack-tip surfaces presumably resulting in decreased bond strengths at the fatigue crack tip, 2) for pressures greater than 10^{-1} Pa, accelerated da/dN in oxygen may result from oxidation at the crack tip limiting reversible slip, and 3) in water vapor, absorption of atomic hydrogen at the reactive crack tip resulting in process zone embrittlement.

14. SUBJECT TERMS

Ti 6-2-2-2-2; corrosion fatigue; titanium alloys; fatigue crack growth; environmentally assisted cracking; gaseous effects

15. NUMBER OF PAGES

32

16. PRICE CODE

A03

17. SECURITY CLASSIFICATION OF REPORT	18. SECURITY CLASSIFICATION OF THIS PAGE	19. SECURITY CLASSIFICATION OF ABSTRACT	20. LIMITATION OF ABSTRACT
Unclassified	Unclassified	Unclassified	UL